N82 23466

# Numerical methods and calculations for droplet flow, heating and ignition

H. A. Dwyer*, B. R. Sanders
D. Dandy†

Sandia National Laboratories
Livermore, California 94550

## Abstract

A new numerical method has been devised and employed to solve a variety of problems related to liquid droplet combustion. The basic transport equations of mass, momentum and energy have been formulated in terms of generalized nonorthogonal coordinates, which allows for adaptive griding and arbitrary particle shape. In this paper example problems are solved for internal droplet heating, droplet ignition and high Reynolds number flow over a droplet.

## Introduction

This paper presents initial results of a research effort whose end goals are the calculation of single and multiple liquid droplet combustion flows. The complete problem of even single droplet combustion presents a severe challenge for present day numerical methods because of the multiple space and time scales which can be introduced into the problem. These scales are the result of high Reynolds and Peclet numbers as well as flame formation around the droplet. In order to resolve all the physical phenomena that are contained in the problem, it is necessary to use the grid points in a numerical solution method very efficiently. A major new advance in the efficient location of grid points is the use of generalized nonorthogonal coordinates and adaptive grids.[1,2,3] It will be shown, and has been shown, that these methods greatly enhance the ability to calculate complex flows.

In the present paper major simplifications have been made in the flow equations to isolate physical phenomena and test the efficiency of the numerical methods employed. The most limiting simplification will be that of constant overall density, however as will be shown, the numerical significance of the results are not damaged by the assumptions made.

## Basic transport equations

The equations for momentum, energy, and mass transport will now be written in terms of generalized coordinates, and the numerical methods employed discussed. The starting point is the equations in terms of axially-symmetric cylindrical coordinates, and the equations for stream function ($\psi$), vorticity ($\omega$), temperature ($T$) and reactant species density ($\rho_a$), which are the following:

$$\frac{\partial}{\partial z}\left(\frac{1}{r}\frac{\partial \psi}{\partial z}\right) + \frac{\partial}{\partial r}\left(\frac{1}{r}\frac{\partial \psi}{\partial r}\right) = \omega \tag{1}$$

$$\frac{\partial}{\partial t}(\rho r\omega) + \frac{\partial}{\partial r}(\rho rv\omega) + \frac{\partial}{\partial z}(\rho ur\omega) - \rho v\omega = \frac{\partial}{\partial r}\left(r\frac{\partial}{\partial r}(\mu\omega)\right) + \frac{\partial}{\partial z}\left(r\frac{\partial}{\partial z}(\mu\omega)\right) - \frac{\mu\omega}{r} \tag{2}$$

$$\text{where } u = -\frac{1}{r}\frac{\partial \psi}{\partial r} \text{ and } v = \frac{1}{r}\frac{\partial \psi}{\partial z} \tag{3}$$

$$\frac{\partial}{\partial t}(\rho rC_p T) + \frac{\partial}{\partial r}(\rho rC_p vT) + \frac{\partial}{\partial z}(\rho rC_p uT) = \frac{\partial}{\partial r}\left(rk\frac{\partial T}{\partial r}\right) + \frac{\partial}{\partial z}\left(rk\frac{\partial T}{\partial z}\right) + r\rho_a \Delta h_a K_a e^{-E_a/RT} \tag{4}$$

$$\frac{\partial}{\partial t}(r\rho_a) + \frac{\partial}{\partial r}(rv\rho_a) + \frac{\partial}{\partial z}(ru\rho_a) = \frac{\partial}{\partial r}\left(rD_a\frac{\partial \rho_a}{\partial r}\right) + \frac{\partial}{\partial z}\left(rD_a\frac{\partial \rho_a}{\partial z}\right) - r\rho_a K_a e^{-E_a/RT} \tag{5}$$

---

*Professor, Department of Mechanical Engineering, University of California Davis.

†Current address, Department of Chemical Engineering, California Institute of Technology, Pasadena, California 91103.

Research supported by U.S. Department of Energy, Office of Basic Energy Sciences, Division of Engineering, Mathematical and Geosciences.

where the following notation has been used for physical constants: $K_a$-pre-exponential reaction constant; $E_a$-activation energy; R-gas constant; k-thermal conductivity, $\rho$-overall density; and $\Delta h_a$-chemical heat release. Also, the independeht variables t, r and z are the time, radial coordinate and axial position, respectively. (A more detailed explanation of the chemical reaction terms will be given later in the paper.)

A major difficulty with the above formulation is that the surface of the droplet does not lie naturally on a constant value of the independent variables r and z. However, this difficulty can be removed immediately by transforming to generalized nonorthogonal coordinates $\xi$, $\eta$, and thereby making the droplet surface correspond to $\eta=0$. In order to simplify notation it will first be useful to rewrite equations (1) through (5) in a vector form

$$\frac{\partial \hat{Q}}{\partial t} + \frac{\partial \hat{E}}{\partial r} + \frac{\partial \hat{F}}{\partial z} = \frac{\partial \hat{R}}{\partial r} + \frac{\partial \hat{S}}{\partial z} + \hat{H} \tag{6}$$

where

$$\hat{Q} = \begin{pmatrix} 0 \\ \rho r\omega \\ \rho r C_p T \\ r\rho_a \end{pmatrix} \qquad \hat{E} = \begin{pmatrix} 0 \\ \rho rv\omega \\ \rho rv C_p T \\ rv\rho_a \end{pmatrix} \qquad \hat{F} = \begin{pmatrix} 0 \\ \rho ru\omega \\ \rho ru C_p T \\ ru\rho_a \end{pmatrix}$$

$$\hat{R} = \begin{pmatrix} \frac{1}{r}\frac{\partial \psi}{\partial r} \\ r\frac{\partial}{\partial r}[\mu\omega] \\ rk\frac{\partial T}{\partial r} \\ rD_a\frac{\partial \rho_a}{\partial r} \end{pmatrix} \qquad \hat{S} = \begin{pmatrix} \frac{1}{r}\frac{\partial \psi}{\partial z} \\ r\frac{\partial}{\partial z}[\mu\omega] \\ rk\frac{\partial T}{\partial z} \\ rD_a\frac{\partial \rho_a}{\partial z} \end{pmatrix} \qquad \hat{H} = \begin{pmatrix} -\omega \\ -\frac{\mu\omega}{r} + \rho v\omega \\ r\rho_a \Delta h_a K_a e^{-E_a/RT} \\ -r\rho_a K_a e^{-E_a/RT} \end{pmatrix}$$

Transforming to the variables $\tau$, $\xi$ and $\eta$ equation (6) becomes

$$\frac{\partial \hat{Q}}{\partial t} + \frac{\partial \hat{F}}{\partial \xi} + \frac{\partial \hat{F}}{\partial \eta} = \frac{\partial \hat{R}}{\partial \xi} + \frac{\partial \hat{S}}{\partial \eta} + \hat{H} \tag{7}$$

where the following new vectors have been defined

$$\hat{Q} = \frac{\hat{Q}}{J}$$

$$\hat{E} = \frac{1}{J}(\hat{Q}\xi_t + \hat{E}\xi_r + \hat{F}\xi_z)$$

$$\hat{F} = \frac{1}{J}(\hat{Q}\eta_t + \hat{E}\eta_r + \hat{F}\eta_z)$$

$$\hat{R} = \frac{1}{J}(\hat{R}\xi_r + \hat{S}\xi_z)$$

$$\hat{S} = \frac{1}{J}(\hat{R}\eta_r + \hat{S}\eta_z)$$

$$\hat{H} = \frac{\hat{H}}{J}$$

and the transformation metrics, or areas and volumes, are given by

$$J = \frac{1}{z_\xi r_\eta - z_\eta z_\xi}$$

$$\xi_z = J r_\eta \qquad \xi_r = - J z_\eta \qquad \xi_t = - z_t \xi_z - r_t \xi_r$$

$$\eta_z = - J r_\xi \qquad \eta_r = J z_\xi \qquad \eta_t = - z_t \eta_z - r_t \eta_r$$

It can easily be seen that the resulting equations are more complex, however the digital computer is extremely well equipped to handle this type of algebraic complexity, and with some additional programming a much more valuable research tool is obtained. The equations as they are written in (7) will easily handle arbitrary-shaped particles as well as particles whose shape is changing as a function of time. However, the major advantage of the above formulation is that it allows the use of adaptive grid procedures to be employed, and this feature will be shown to be one of the single most important advances in the efficient use of numerical methods to solve complex physical problems.

An interesting feature of these equations is that they allow for the use of variable transport properties $\mu$, $k$ and $D_a$, although the overall density must be constant. To the authors' knowledge this is the first time that a variable transport property formulation of the stream function-vorticity equations has been given. This formulation will be a complete description of the mass and energy transport processes inside the droplet, where constant overall density is assumed.

## Numerical methods

The original plan for the numerical solution method was to employ a fully implicit iterative scheme to solve the set of transport equations given previously. In order to solve these equations an alternating-direction-implicit[4] (ADI) scheme was employed together with a Newton procedure to linearize the equations where necessary[5]. The resulting equations are block tridiagonal, and the efficient solver of Hindmarsh[5] was used to obtain the solution. This procedure proved to be unstable because of the large sensitivity that the stream function has to all errors. The coupling of the vorticity and stream function equations, plus generalized coordinates, and block solutions along a line, causes the truncation error to give very inaccurate values of stream function near the boundary. A major part of the problem is due to the fact that the stream function can change by four or five orders of magnitude from the body surface to the free stream. The values of the stream function near the surface are very small and truncation error in the outer part of the flow overwhelms the small stream function values near the surface. The solution to the problem is point relaxation of the stream function equation on a previously calculated vorticity distribution, followed by iteration between the stream function and vorticity equations. This point relaxation method does not couple all the truncation errors together, and very good results were obtained.

The numerical method that was finally employed had the following features:

I. Stream function-vorticity equations
   a. First-order backward, implicit time differences for time derivatives.
   b. Second-order central differences in space.
   c. ADI solution of the vorticity equation.
   d. Point relaxation of the stream function equation.
   e. Global iteration on both equations.

II. Energy and species equations
   a. The same space and time differencing as the vorticity equation.
   b. Newton linearization of the nonlinear terms.
   c. Block tridiagonal solution with an ADI marching technique.

The above numerical method is somewhat ad hoc in that it uses two difference methods within itself to determine a solution, however the individual methods reflect the numerical nature of the equations being solved. The block tridiagonal solution of the energy and species equation is excellent for chemical reactions, while the point iteration method allows the stream function to converge accurately and smoothly on the vorticity distribution.

## Criterion for grid placement

The basic criterion for grid placement that was employed in the present paper will now be presented. The computational space, $\xi$ and $\eta$, has been normalized so that their numerical values go between zero and one, and the grid points are fixed in time. In the physical

space the grid points will be placed and moved in time to achieve the resolution of high gradient regions. Along a given arc in the physical space the grid points will be distributed in proportion to the gradient of the dependent variable. If the distance along a given arc in physical space is denoted by S, a mathematical statement of the relationship between the computational and physical space is

$$d\xi \propto \left|\frac{\partial T}{\partial s}\right| ds$$

where S is the distance measured on the $\eta$ = constant arc, and T the dependent variable of the transport equation being solved, in this paper the dependent variable is temperature. In order to normalize, allow for "optimization," and remove singularities, the above equation is cast into the following form

$$\xi(x,y,t) = \frac{\left[\int_0^S \left(1 + b\left|\frac{\partial T}{\partial s}\right|\right) ds\right]}{\left[\int_0^{S_{max}} \left(1 + b\left|\frac{\partial T}{\partial s}\right|\right) ds\right]}$$

where b is an adjustable constant used for "optimization" of the grid distribution.

The above equation has some interesting features which will now be discussed briefly. For the case b = 0 a uniform distribution of points on the nonorthogonal arc is obtained, while for large b, constant values of the variable T, or isotherms, are selected. The coordinate location equation is solved in an explicit sense at the old time step, and the details can be found in the paper by Dwyer et al.[2] Also, it should be mentioned that the accuracy in solving the equation does not influence directly the accuracy of the finite difference solution. With the use of these generalized coordinates and an adaptive grid technique a powerful new method is available for numerical solution.

In the present paper the adaptive griding procedure has only been employed in the calculation of the temperature and species concentrations, and has not been used for the stream function-vorticity part of the method. The stream function and vorticity have been calculated from a predetermined grid, however the use of adaptive griding for the fluid dynamics is being implemented at the present time.

## Results

The results which will be presented illustrate mainly the capability of the calculation method, and do not give a complete description of droplet combustion. The problems which have been solved are the following:

1. Ignition and flame propagation about hot particles.
2. Separated flow around liquid droplets.

A description of each of these results will now be given.

The first problem solved was to calculate the ignition and flame propagation about a spherical particle. The reaction mechanism is very simple and consisted of a premixed fuel A reacting and going over to species B. The nondimensional form of the energy and species equations are

$$\frac{D\hat{T}}{Dt} = \frac{1}{Pe}\frac{1}{\partial x_i}\left(\frac{\partial \hat{T}}{\partial x_i}\right) + \hat{\rho}_a N_{DA} e^{-\theta_a/\hat{T}}$$

$$\frac{D\hat{\rho}_a}{Dt} = \frac{1}{Pe}\frac{\partial}{\partial x_i}\left(\frac{\partial \hat{\rho}_a}{\partial x_i}\right) - \hat{\rho}_a N_{DA} e^{-\theta_a/\hat{T}}$$

where $Pe = \frac{U_\infty d}{\alpha}$ Peclet Number, based on maximum velocity $U_\infty$ inside the droplet

$N_{DA}$ = Dimensionless Pre-Exponential Reaction Coefficient.

$\theta_a$ = Activation Temperature, $E_a/R$.

and it has been assumed that all transport coefficients are constant, and that the thermal diffusivity and species diffusivity are equal.

For this ignition model problem the velocity field was assumed to be that given by Stokes flow, and the overall density was assumed constant. The value for the Peclet number was chosen to be 200 and $\theta_a$=4 for an initial temperature of premixed reactant of $\hat{T}$=.2. The spherical particle surface will be raised impulsively to $\hat{T}$=1.0 and the adiabatic flame temperature in terms of dimensionless temperature is $\hat{T}_{AD}$ = 1.2.

The values for the pre-exponential coefficient were chosen to be characteristic of hydrocarbon fuels, thus the basic time scales of the processes are similar to a moderate Reynolds number particle in a premixed hydrocarbon gas (however, the simulation is highly simplified as can be easily seen). The first results for the numerical simulation are shown in Figures (1) through (4) for $N_{DA} = 2.2 \cdot 10^5$, which corresponds to a rather thin flame compared to particle diameter. Figures (1) and (2) show the coordinate system (top) and isotherm distribution for a uniform grid simulation. A careful study of the isotherm distribution shows oscillations in the flame, and this is due to the high cell Peclet numbers.

The oscillations are more severe as the flame moves away from the body, because of the natural increase in grid cell size occurring in spherical coordinates. As the flame approaches the computational boundary there is only one point to describe the flame structure. This lack of resolution results in temperature and species oscillations in the calculation, incorrect flame speed and eventually termination of the calculation due to negative values of temperature and species.

A second more accurate calculation with the same number of grid points, but with the adaptive grid strategy employed is shown in Figures (3) and (4). The most dramatic feature of the calculation is the bunching of the grid points inside the flame structure. This removes all the numerical oscillations, and the overall flame speed agrees well with the results of Otey and Dwyer.[10] The results of this calculation thus show dramatically the usefulness and capabilities of the adaptive grid procedure for combustion problems.

A second calculation with a reduced reaction rate ($N_{DA} = 2.2 \cdot 10^3$) is shown in Figures (5) through (8). In this case the flame is much thicker and the coordinate adaption is only very slight. However, the ignition and flame propagation processes are much more interesting. Figure (5) exhibits the isotherm distribution at an early time with a maximum temperature of $\hat{T}$ = 1.0 occuring at the particle surface. As time increases an ignition process occurs at the rear stagnation point (Figure (6)) and then a steady state reaction zone is set up on the leeward side of the particle (Figures (7)-(8)). It is easily seen from the isotherm distribution that the surface location where the gas temperature rises above the wall temperature quickly stabilizes on the leeward side of the particle surface. These results show that the present calculation methods will resolve ignition phenomena in particle dynamics.

The final results to be presented are a demonstration of the ability of the numerical methods to calculate the fluid flow around and inside droplets. Shown in Figures (9) through (11) are the distribution of stream function and vorticity for a solid particle in a flow with a Reynolds number of 100, based on particle diameter. Figure (9) exhibits the distribution of stream function outside the particle, while Figure (10) shows the stream function inside the separation bubble (the top figure is the coordinate distributions). A more dramatic representation of high Reynolds number influences can be seen in Figure (11) where the normalized vorticity contours are given. The bunching of the contours on the windward side of the particle is clear evidence of the start of boundary layer formation and separation.

All of the above results agree well with the calculations of Le Clair.[7] Figure (12) exhibits the streamline pattern inside of a liquid droplet at an external flow Reynolds number of 200. For this calculation the ratios of liquid droplet to gas viscosity and density are respectively

$$\frac{\mu_\ell}{\mu_g} = 50 \qquad \frac{\rho_\ell}{\rho_g} = 1000$$

which are typical values of interest to combustion problems. Therefore, it seems that the methods we are employing are quite encouraging, and give strong promise of giving new results for the complete problem of droplet combustion.

## Conclusions

A new collection of numerical techniques has been assembled to solve problems of heat, mass and momentum transport in droplet combustion systems. The major new features of this collection of methods are the following:

1. Generalized Nonorthogonal Coordinates
2. Adaptive Griding on Temperature Gradients
3. Block Tridiagonal Solution of Energy and Species Equations
4. Point Iteration of the Stream Function on the Vorticity Distribution

All of the above methods have shown themselves stable and capable of giving improved results for the fluid flow, heat transfer, and mass transfer problems solved.

The physical problems solved in the paper were moderate Reynolds number flow over both solid and liquid droplets, as well as a study of ignition around a hot solid particle in a Stokes flow. The fluid flow studies reproduced the results of other investigators, and thus verified the accuracy of the methods employed. The study of ignition about a hot particle showed clearly that ignition can be delayed until the leeward side of the particle, and a flame can be stabilized in the wake of the particle. These results seem to be new, and the future inclusion of variable density will allow for a complete description of particle ignition. Also, it should be mentioned again that the high-reaction-rate ignition studies would not be possible without adaptive griding, because of its efficient use of grid points.

## References


1. Dwyer, H. A., Kee, R. J., Barr, P. K., and Sanders, B. R. "Transient Droplet Heating at High Peclet Number," A.S.M.E. Winter Annual Meeting, Symposium on Computers and Fluids, November 1981.
2. Dwyer, H. A., Kee, R. J., and Sanders, B. R., "Adaptive Grid Method for Problems in Fluid Mechanics and Heat Transfer," AIAA J., Vol. 18, No. 10, October 1980, p. 1205.
3. Steger, J. L., "Implicit Finite-Difference Simulation of Flow About Arbitrary Two-Dimensional Geometries." AIAA Journal, Vol. 16, July 1978, pp. 679-686.
4. Roache, P., Computational Fluid Dynamics, Hermosa Publishers, Albuquerque, New Mexico, 1971
5. Hindmarsh, A. C., "Solution of Block-Tridiagnonal Systems of Linear Algebraic Equations," Report UCID-30150, Lawrence Livermore Laboratory, February 1977.
6. Otey, G. and Dwyer, H. A., "A Numerical Study of the Interaction of Fast Chemistry and Diffusion," AIAA J., Vol. 17, June 1979, pp. 606-613.
7. Le Clair, B. P., Hamielec, A. E., Pruppacher, H. R. and Hall, W. D., "A Theoretical and Experimental Study of the Internal Circulation in Water Drops Falling at Terminal Velocity in Air, Journal of Atmospheric Sciences, V. 29, pp. 728-740.

ORIGINAL PAGE
BLACK AND WHITE PHOTOGRAPH

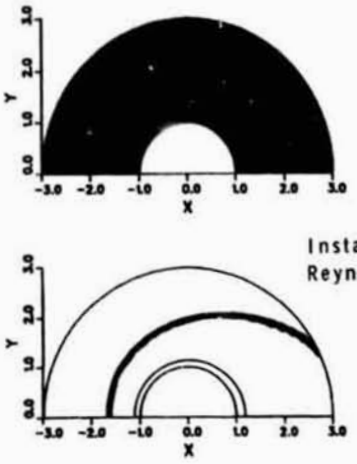


Fig. 1. Flame propagation with a uniform grid, $N_{DA} = 2.2 \cdot 10^5$.

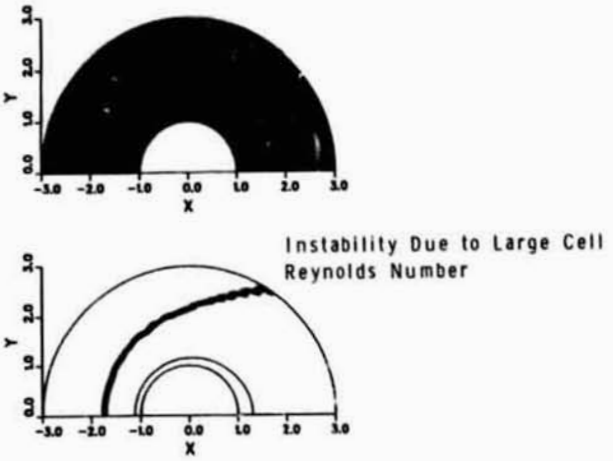


Fig. 2. Flame propagation with a uniform grid, $N_{DA} = 2.2 \cdot 10^5$.

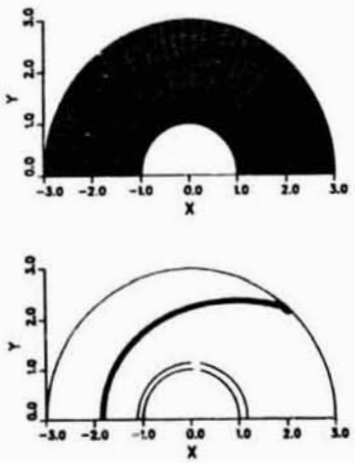


Fig. 3. Flame propagation with an adaptive grid, $N_{DA} = 2.2 \cdot 10^5$.

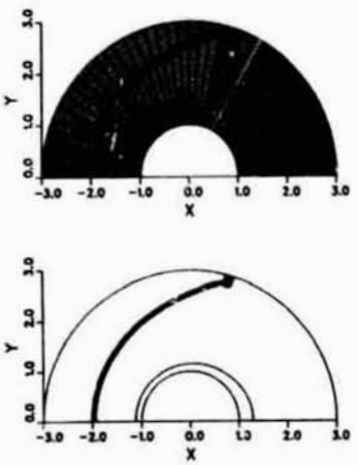


Fig. 4. Flame propagation with an adaptive grid, $N_{DA} = 2.2 \cdot 10^5$.

$\tau = \frac{\alpha t}{R^2} = 0.04$

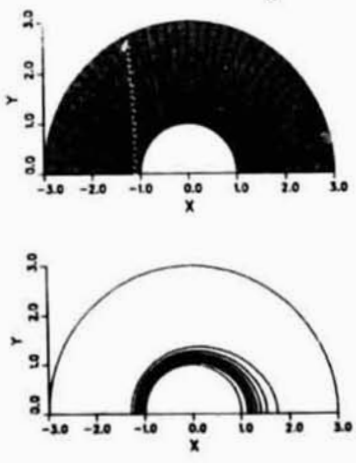


Fig. 5. Preignition isotherm distribution.

$\tau = \frac{\alpha t}{R^2} = 0.06$

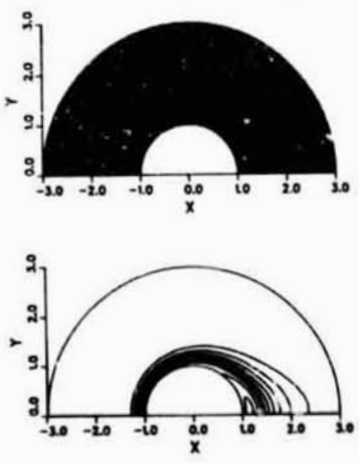


Fig. 6. Ignition isotherm distribution.

ORIGINAL PAGE
BLACK AND WHITE PHOTOGRAPH

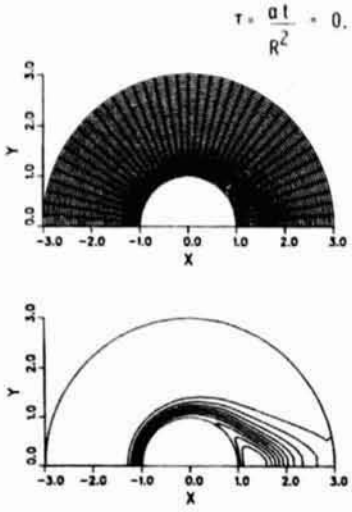


Fig. 7. Postignition isotherm distribution.

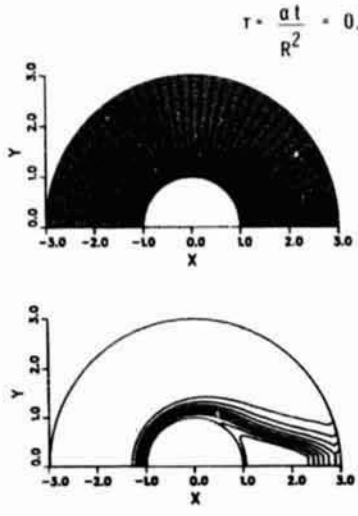


Fig. 8. Postignition isotherm distribution.

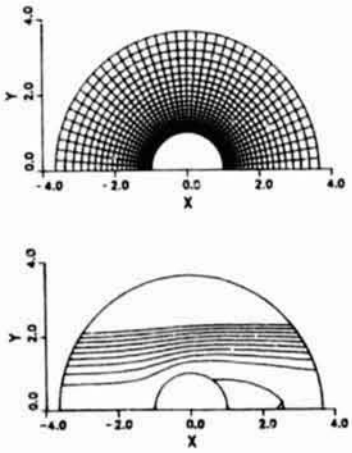


Fig. 9. External streamlines; solid particle, Re = 50.

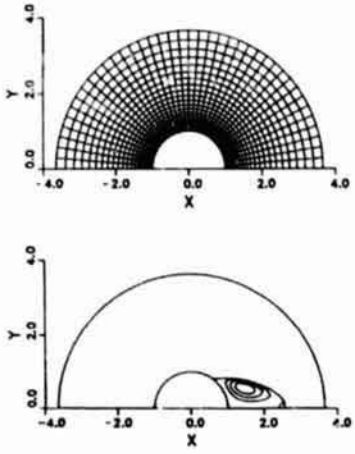


Fig. 10. Separation bubble streamlines; solid particle, Re = 50.

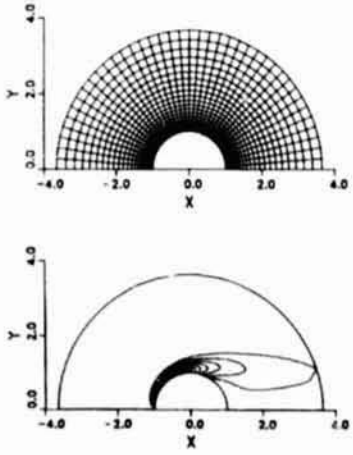


Fig. 11. Vorticity distribution; solid particle, Re = 50.

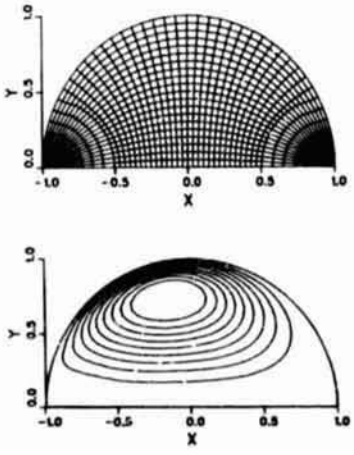


$P_\ell/Pa = 1000$

$\mu_\ell/\mu a = 50$

Fig. 12. Streamline distribution; liquid droplet, Re = 100.